Al-Qadisiyah Journal of Pure Science

ISSN(Printed): 1997-2490 ISSN(Online): 2411-3514

DOI: 10.29350/jops

Al-Qadisiyah Journal of Pure Science

Micellar Systems Loaded with Iron Oxide Nanoparticles: Rheological and Thermodynamic Evaluation for Potential Drug Delivery Applications

[1]Tamara Adndn Jawad، [2]Diana Abdul Karim ، [3]Laqa'a Hussein Alwan

[1] Samarra University, College of Education, Department of Chemistry

[1]Corresponding author: eduhm250012@stu.uosamarra.edu.iq

[2]deyana.Abd@ uosamarra.edu.iq

[3]Liqaa.h@uosamarra.edu.iq

Received: 03/05/2026; Accepted: 08/05/2026; Published Online: 08/05/2026.

Abstract

This study explores the preparation and characterization of mixed surfactant systems composed of cetyltrimethylammonium bromide (CTAB) and sodium dodecylbenzene sulfonate (SDBS) at various ratios and temperatures (283–313 K). Iron oxide (Fe_3O_4) nanoparticles were synthesized via a green method and characterized using FT-IR, SEM, EDX, and TEM, confirming their morphology, composition, and nanoscale structure. Rheological analysis revealed that the CTAB:SDBS (7:3) ratio exhibited the highest viscosity, ranging from 0.0018 to 0.0260 × 10^2 Pa•s. Thermodynamic evaluation indicated spontaneous micellization ($\Delta G°$ = −2.25 to −4.40 kJ•mol^{-1}) and an exothermic process (ΔH = −67.270 kJ•mol^{-1}), with negative entropy values. The incorporation of amoxicillin enhanced viscosity, reaching 0.0325 × 10^2 Pa•s at 200 ppm, while maintaining spontaneous and exothermic behavior. The combined system containing CTAB:SDBS (7:3), amoxicillin, thyme extract, and Fe_3O_4 nanoparticles demonstrated the highest viscosity (0.0372 × 10^2 Pa•s) and activation energy (0.812 kJ•mol^{-1}). Thermodynamic parameters confirmed stable and spontaneous micelle formation. Overall, the results highlight the potential of these mixed micellar systems as efficient drug delivery platforms.

keywords: Iron oxide nanoparticles (Fe_3O_4), Micelle formation, promising micellar carrier, amoxicillin, green synthesis, thermodynamic parameters.

Introduction:

Nanoscience is a multidisciplinary research field that studies materials and structures at the nanoscale (typically 1–100 nm), where the physical and chemical properties of matter change due to the extremely small size, enabling the design of materials and systems with unique features [1]. In recent decades, nanoscience and nanotechnology have become central to advances in materials science and manufacturing technologies through the precise control of matter at the nanometer scale (10^{-9} m) [2]. Nanomaterials exhibit unique properties compared with their bulk counterparts, including a high surface-to-volume ratio, enhanced mechanical strength, improved electrical and thermal properties, and quantum effects that provide novel functionalities [3,4]. These features have promoted their use in numerous biomedical and industrial applications. In nanomedicine, nanotechnology has enabled the development of advanced potential drug delivery systems capable of selectively targeting specific cells and tissues, thereby improving drug bioavailability and therapeutic efficiency. Amoxicillin, a semi-synthetic β-lactam antibiotic, is widely used against Gram-positive and some Gram-negative bacteria [5]. In addition, natural products such as thyme extract contain bioactive compounds, including thymol and carvacrol, which possess important pharmacological activities [6]. Potential Drug delivery systems can also be enhanced using nanomaterials such as iron oxide nanoparticles (Fe_3O_4NPs), which exhibit high surface area and efficient interaction with biological tissues [7]. These nanocarriers improve targeted drug delivery to sites such as tumors and inflamed tissues while reducing adverse side effects associated with conventional therapies[8] .Fig. (1) illustrates the importance of nanomaterials in potential drug delivery systems. Surfactants are widely used in pharmaceutical, chemical, and nanotechnological applications because of their ability to reduce surface and interfacial tension between different phases, such as water–oil and water–air systems [9]. Their amphiphilic structure, containing both hydrophilic and hydrophobic moieties, enables adsorption at interfaces and modification of physicochemical properties. Above the critical micelle concentration (CMC), surfactant molecules self-assemble into nanosized micelles, where the hydrophobic groups orient inward and the hydrophilic groups outward, thereby enhancing stability in aqueous media. [10]. Surfactants are classified according to the charge of their polar head groups into cationic, anionic, nonionic, and zwitterionic types. For example, cetyltrimethylammonium bromide (CTAB) is one of the most prominent cationic surfactants belonging to quaternary ammonium compounds, with the structural formula (CH_3–$(CH_2)_{15}$–$N^+(CH_3)_3$ Br^-), while sodium dodecylbenzene sulfonate (SDBS) is a well-known anionic surfactant with the structural formula ($C_{12}H_{25}$–C_6H_4–SO_3Na). Each type exhibits distinct physicochemical properties that determine its applications [11]. **Fig (2)** illustrates the classification of

surfactants. These compounds have significantly contributed to the advancement of pharmaceutical industries, where they are used to improve the solubility of poorly water-soluble drugs, enhance bioavailability, and reduce side effects [12]. Moreover, they play a key role in the preparation and stabilization of nanoparticles by preventing aggregation, and they are essential components in the design of advanced potential drug delivery systems, including micellar and nanoscale carriers, making them indispensable in modern nanotechnology and targeted therapeutic applications [13].

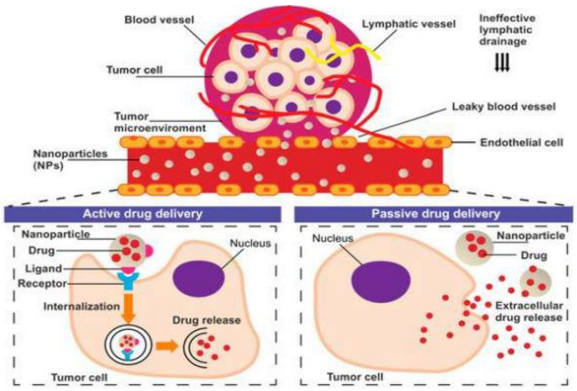

Fig (1). illustrates the role of nanomaterials in drug delivery systems [14].

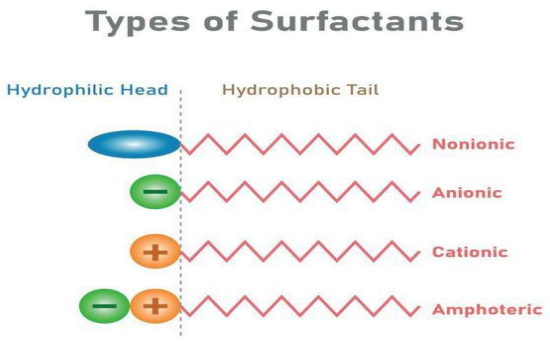

Fig (2). illustrates the classification of surfactants [15].

Materials and Methods:

Preparation of Surfactant Solutions (SDBS and CTAB):

Stock solutions of cetyltrimethylammonium bromide (CTAB) and sodium dodecylbenzene sulfonate (SDBS) were prepared at a concentration of 3 wt%. This was achieved by dissolving 3.1 g of each surfactant separately in deionized distilled water in a 100 mL volumetric flask, followed by dilution to the mark with the same solvent. The solutions were thoroughly agitated to ensure complete dissolution. Mixed surfactant systems were then prepared by combining appropriate volumes of the CTAB and SDBS stock solutions to obtain different mixing ratios. The final volume of each prepared mixture was adjusted to 10 mL. This procedure allowed the preparation of solutions with varying composition ratios of the two surfactants. The specific volumes withdrawn from the stock solutions to prepare each mixture are presented in **Table (1)**, and the preparation scheme is illustrated in **Fig (3)** .

Table (1): Volumes withdrawn from the stock solutions of the surfactants.

Sample	**A_1**	**A_2**	**A_3**	**A_4**	**A_5**	**A_6**	**A_7**	**A_8**	**A_9**	**A_{10}**	**A_{11}**
CTAT	10	9	8	7	6	5	4	3	2	1	0
SDBS	0	1	2	3	4	5	6	7	8	9	10
V.total	10	10	10	10	10	10	10	10	10	10	10

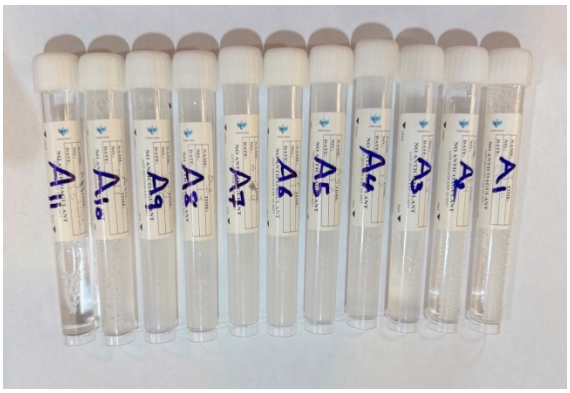

Fig (3): Arrangement of the prepared mixture samples after preparation.

Preparation of Amoxicillin Solution and Standard Solutions

A 100 mL stock solution of amoxicillin at a concentration of 500 ppm was prepared by dissolving 0.047 g of amoxicillin in an appropriate amount of deionized water in a 100 mL volumetric flask. The solution was then diluted

to the mark with deionized water and thoroughly shaken to ensure complete dissolution. From this stock solution, a series of diluted solutions with different concentrations (200, 100, 50, and 25 ppm) were prepared, each with a final volume of 100 mL, using the dilution equation. These solutions were subsequently used for mixing with different volumes of CTAB and SDBS solutions to investigate their viscosity behavior.

Preparation of Thyme Extract [16].

Thyme extract was prepared using the maceration method with deionized water as the solvent, following the steps below:

1. Ten grams of dried thyme were washed three times with deionized water and dried in an oven for 30 minutes to remove impurities.
2. The dried plant material was ground and transferred into a 100 mL beaker, then 50 mL of deionized water was added. The mixture was heated at 50 °C with continuous stirring.
3. The resulting mixture was filtered to obtain the crude plant extract.
4. The filtrate was dried in an oven at 60 °C until complete evaporation of the solvent.
5. A mass of 0.5 g of the dried extract was dissolved in a 100 mL volumetric flask to prepare a 500 ppm stock solution, from which further dilutions were prepared as needed.

Preparation of Iron Oxide Nanoparticles (Fe_3O_4)

Fe_3O_4 nanoparticles were synthesized via a green synthesis approach [17]. Initially, 6.5 g of $FeCl_3 \cdot 6H_2O$ and 4.5 g of $FeCl_2 \cdot 4H_2O$ were dissolved in deionized water at a molar ratio of 2:1 under constant stirring. Subsequently, 50 mL of grape juice extract was added gradually in five portions (10 mL each), with a 10-minute interval between additions. The mixture was heated at 85 °C for 2.5 hours under continuous magnetic stirring. Upon addition of 50 mL of 0.5 M NaOH solution dropwise, the pH was adjusted to 9, resulting in a color change from light green to black, indicating nanoparticle formation. The resulting suspension was centrifuged at 10,000 rpm to collect the precipitated nanoparticles. The solid product was washed several times with ethanol and deionized water to remove residual impurities and

unreacted species. Finally, the obtained nanoparticles were dried in an oven at 60 °C to yield the Fe_3O_4 nanoparticle powder, as shown in **Fig (4)**. as represented by the following equation.

$$FeCl_2.4H_2O + 2FeCl_3.6H_2O + 8NaOH \longrightarrow Fe_3O_4 \downarrow + 8NaCl + 20H_2O$$

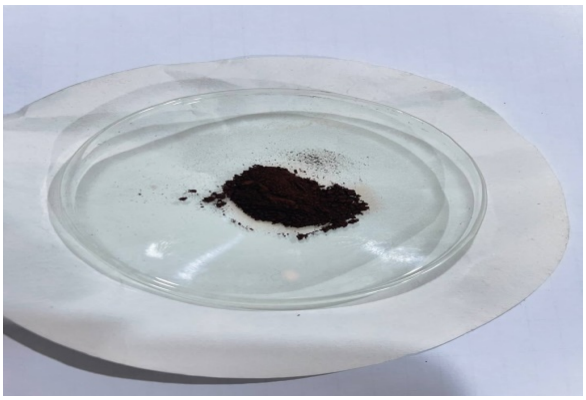

Fig (4): Iron oxide nanoparticles (Fe_3O_4) prepared via the green synthesis method.

Viscosity Measurements

The water bath was adjusted to the required temperatures, and the viscometer along with the sample holder was immersed in the bath, ensuring partial submersion. The system was left for 5 minutes to reach thermal equilibrium, with intermittent stirring to maintain uniform temperature distribution. The efflux time was measured using an Ostwald viscometer, as illustrated in **Fig (5)**, by recording the time required for the solution to flow between the marked start and end points on the instrument. Each measurement was repeated five times, and the average flow time was calculated for accuracy. This procedure was carried out at four different temperatures (283, 293, 303, and 313 K) and applied to all prepared surfactant mixture samples . The viscosity was calculated using Poiseuille–Ostwald equation as follows [18]:

$$\frac{\eta_1}{\eta_2} = \frac{\sigma_1 t_1}{\sigma_2 t_2} \quad (1)$$

where:

- σ_1: density of water (g/cm³)
- t_1 : flow time of water (s)

- η_1 : viscosity of water (Pa·s)
- σ_2: density of the sample (g/cm³)
- t_2: flow time of the sample (s)
- η_2 : viscosity of the sample (Pa·s)

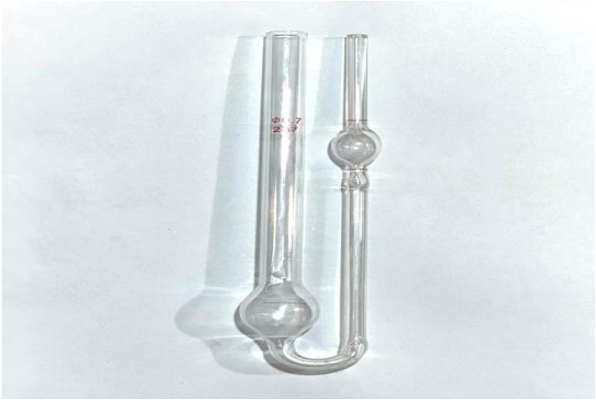

Fig (5): Ostwald viscometer used for viscosity measurements.

Preparation of CTAB:SDBS Mixed Solutions with Different Amoxicillin Concentrations

Four mixed surfactant solutions with a fixed ratio of 7:3 (CTAB:SDBS) were prepared. These mixtures were formulated in the presence of different amoxicillin concentrations (200, 100, 50, and 25 ppm), with a final total volume of 10 mL for each sample. The required volumes of the prepared CTAB and SDBS stock solutions were accurately measured and mixed to obtain the desired surfactant ratio for each drug concentration. The detailed volumes of the surfactant solutions used in each prepared sample are presented in Table (2). The prepared samples arrangement, labeled from B1 to B4, after preparation is illustrated in **Fig (6)** .

Table (2): Volumes of CTAB and SDBS solutions used in the preparation of samples at different amoxicillin concentrations.

Sample Code	**B_1**	**B_2**	**B_3**	**B_4**
V(SDBS) + (CTAB)	9	9	9	9
Conc. Amoxi	25	50	100	200
V Amoxi	1	1	1	1
V.total	10	10	10	10

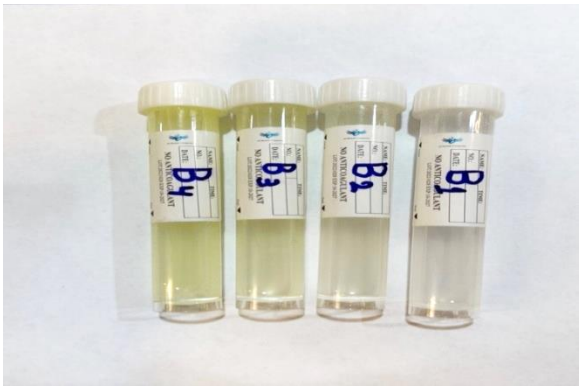

Fig (6): Arrangement of the prepared mixture samples after preparation.

Preparation of Surfactant Mixtures in the Presence of Iron Oxide Nanoparticles, Amoxicillin, and Thyme Extract

A 100 mL stock solution of iron oxide nanoparticles (Fe_3O_4) at a concentration of 500 ppm was prepared by dissolving 0.05 g of the nanoparticles in an appropriate amount of deionized water in a 100 mL volumetric flask, and the volume was then completed to the calibration mark with the same solvent. From this stock solution, a series of diluted solutions with concentrations of 200, 100, 50, and 25 ppm were prepared using the dilution method. Subsequently, 1 mL of each nanoparticle concentration was added to a surfactant mixture with a fixed volume ratio of 7:3 (SDBS:CTAB), in the presence of amoxicillin and thyme extract. The final volume of each prepared system was adjusted to 10 mL. The detailed compositions of the prepared mixtures are presented in Table (3). The arrangement and labeling of the prepared samples (D1–D4) after preparation are illustrated in **Fig (7)**.

Table (3): Volumes of CTAB and SDBS solutions used in the presence of amoxicillin, thyme extract, and different concentrations of iron oxide nanoparticles.

Sample Code	**D_1**	**D_2**	**D_3**	**D_4**
V(SDBS) + (CTAB) (ml)	7	7	7	7
Conc. Amoxi (ppm)	25	50	100	200
V Amoxi (ml)	1	1	1	1
Conc. Thyme (ppm)	25	50	100	200
V Thyme (ml)	1	1	1	1
Conc. Fe_2O_3 (ppm)	25	50	100	200
V Fe_2O_3 (ml)	1	1	1	1
V.total (ml)	10	10	10	10

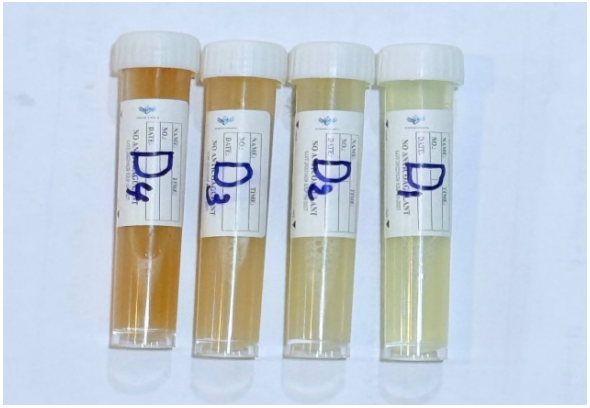

Fig (7): Arrangement of the prepared samples (D1–D4) after preparation. Thermodynamic Parameters for Micelle Formation

Entropy (ΔS°) is a thermodynamic property that represents the degree of randomness within a system. An increase in system randomness corresponds to an increase in entropy. During micelle formation, the disruption of the structured water molecules leads to an increase in entropy. The relationship between the change in entropy (ΔS°) and the change in Gibbs free energy (ΔG°) is given by the following equation [19].

$$G^\circ = H - T\ S^\circ \qquad (2)$$

The enthalpy contribution associated with micelle formation is often relatively small compared with entropy-driven effects. Therefore, an increase in entropy results in a decrease in Gibbs free energy (ΔG°). Processes associated with a decrease in Gibbs free energy occur spontaneously, as it results in a more thermodynamically stable system. Accordingly, micelle formation is considered a spontaneous process. The thermodynamic parameters, including standard Gibbs free energy (ΔG°), enthalpy change (ΔH), entropy change (ΔS°), and activation energy (Ea), can be determined based on viscosity measurements. Viscosity is considered an important indicator for the formation of rod-like and worm-like micelles. The standard Gibbs free energy (ΔG°) was calculated using the following equation [21،20] :

$$G^\circ = RT \ln(/2\times10^{-3}) \qquad (3)$$

where:

- **T**: absolute temperature (K),
- **R**: universal gas constant (8.314 $J \cdot K^{-1} \cdot mol^{-1}$)
- **η**: viscosity of the mixture (Pa·s)

The enthalpy change (ΔH) was determined using the Van't Hoff equation [22].

$$= - \text{Slop} \quad R \qquad (4)$$

where the slope is obtained from the linear plot of ln(η) versus 1/T, as shown in **Fig (8).**

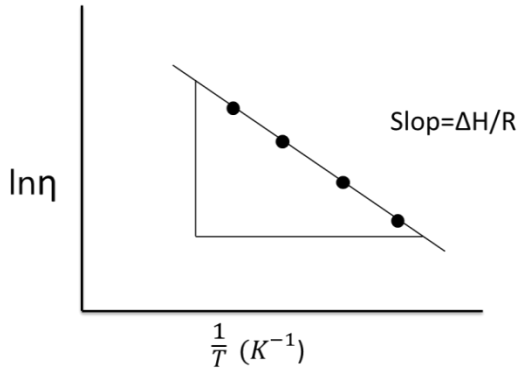

Fig (8): Determination of the slope using the Van't Hoff relationship.

The entropy change (ΔS°) for the micellization process was calculated using the following equation [23].

$$S^\circ = \quad H - \quad G^\circ/T \qquad (5)$$

The activation energy (Ea) can be calculated using the following equation [24].

$$Ea = \text{Slop} \quad R \qquad (6)$$

The slope can be obtained from the plot of viscosity versus the reciprocal of temperature (1/T), as illustrated in **Fig (9).**

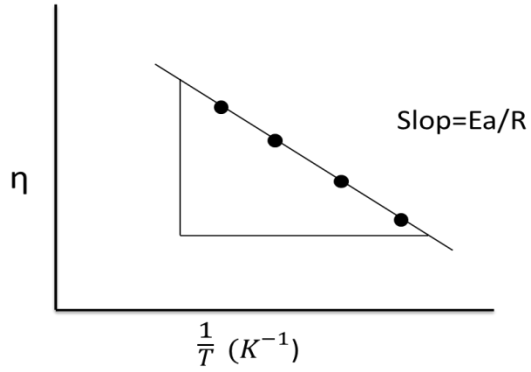

Fig (9): Determination of the slope from the relationship between viscosity and the reciprocal of temperature (1/T).

The formation of micelles in aqueous solutions is a clear example of thermodynamically driven self-assembly processes [25], where aggregation occurs when the system becomes energetically more stable than the individual dispersed molecules. This stability is reflected by a decrease in the Gibbs free energy of the system ($\Delta G^\circ < 0$). Such stabilization arises from a balance between enthalpic contributions, mainly due to attractive interactions among hydrophobic chains, and entropic effects associated with the release of structured water molecules [26]. Micellar structures are dynamic in nature and can vary depending on several factors, including chemical composition, alkyl chain length, head group charge, temperature, and concentration. These factors may induce morphological transitions such as spherical, cylindrical, or lamellar structures, all of which aim to minimize the system's free energy. Moreover, micellar systems are considered stable nanoscale carriers capable of enhancing the solubility and stability of hydrophobic drugs while reducing their toxicity. This makes them a fundamental platform in the design of advanced potential drug delivery systems [13].

Results and Discussion

Viscosity Measurements and Thermodynamic Parameters of Wormlike Micelles in SDBS:CTAB Systems

The formation of wormlike (thread-like) micelles is a significant structural phenomenon that has a direct and pronounced effect on the physicochemical properties of solutions, particularly viscosity. The transition of micelles from spherical to elongated wormlike structures leads to a substantial increase in solution viscosity due to the entanglement of these extended aggregates and the formation of a dynamic three-dimensional network. Therefore, viscosity can be considered a sensitive indirect indicator of wormlike micelle formation [27]. In this context, the present study investigates the ability of a binary surfactant system composed of oppositely charged species, the anionic sodium dodecylbenzene sulfonate (SDBS) and the cationic cetyltrimethylammonium bromide (CTAB), to form wormlike micelles. The electrostatic attraction between oppositely charged head groups is expected to reduce repulsive forces, thereby enhancing self-assembly processes [28]. This interaction facilitates a structural transition from spherical micelles to wormlike micelles at specific mixing ratios and concentrations. The rheological behavior of the system was examined through viscosity measurements at different CTAB:SDBS mixing ratios and at various temperatures (283, 293, 303, and 313 K), in order to evaluate the effect of both composition and temperature on micellar dynamics. The obtained results were correlated with thermodynamic parameters, as the formation of wormlike micelles is associated with a decrease in Gibbs free energy (ΔG°), indicating enhanced thermodynamic stability. In addition, both entropy change (ΔS°) and enthalpy change (ΔH) contribute significantly to defining the spontaneity and nature of micellization [29]. Table (4) presents the calculated viscosity values for a surfactant system containing 3% of both CTAB and SDBS at different mixing ratios and temperatures. The samples are labeled from A1 to A11, providing a quantitative understanding of the relationship between structural arrangement and the physicochemical properties of the system.

Table (4): Viscosity values of CTAB:SDBS surfactant mixtures at different mixing ratios and temperatures.

sample	ctab	sdbs	η(pa.s)× 10^2			
	3%	3%	283 K	293 K	303 K	313 K
A_1	10	0	0.001616	0.001284	0.00098	0.000934
A_2	9	1	0.002507	0.001998	0.001673	0.001161
A_3	8	2	0.009139	0.003274	0.002099	0.001393
A_4	7	3	0.026031	0.010454	0.003021	0.001843
A_5	6	4	0.016797	0.004909	0.002303	0.00176
A_6	5	5	0.010494	0.003206	0.002033	0.001635
A_7	4	6	0.005635	0.002514	0.001764	0.001492
A_8	3	7	0.003708	0.002026	0.001454	0.001237
A_9	2	8	0.002306	0.00161	0.001109	0.001125
A_{10}	1	9	0.001607	0.001191	0.000986	0.001014
A_{11}	0	10	0.001339	0.001062	0.000869	0.000857

The results demonstrated a significant decrease in the viscosity of the studied solutions with increasing temperature. This behavior is mainly attributed to increased molecular kinetic energy, which weakens intermolecular interactions and reduces hydrogen bonding between water molecules, as well as diminishing the strength of interactions between surfactant molecules and water[30]. Consequently, the resistance to flow decreases, leading to a reduction in viscosity. Furthermore, the system containing CTAB exhibited higher viscosity compared to that containing SDBS. This difference is mainly attributed to the longer hydrocarbon chain of CTAB relative to SDBS, which enhances hydrophobic interactions between hydrocarbon chains and contributes to increased viscosity [31]. On the other hand, the results suggest the formation of wormlike micelles within the investigated system, as a significant increase in viscosity was observed at specific mixing ratios between SDBS and CTAB. The maximum viscosity value was recorded at 283 K and a mixing ratio of 7:3 (SDBS:CTAB), reaching 0.02603 × 10^2 Pa·s for sample A4. This increase can be attributed to the formation of elongated and entangled micellar structures, which enhance flow resistance. These findings are consistent with previous studies [32], which reported that binary surfactant systems composed of oppositely charged species tend to form wormlike micelles at specific mixing ratios, resulting in a significant increase in viscosity [33].

Standard Gibbs Free Energy (ΔG°) of SDBS:CTAB Mixtures at Different Mixing Ratios and Temperatures

Micelle formation in aqueous solutions, arising from the self-assembly of surfactant molecules, is a thermodynamically controlled process [34]. Accordingly, a proper description of this phenomenon requires the evaluation of the associated thermodynamic parameters at different temperatures to understand the stability and nature of the formed micellar structures. In this study, the standard Gibbs free energy of micellization (ΔG°) was calculated over the temperature range of 283, 293, 303, and 313 K using Equation (2). Table (5) presents the calculated ΔG° values for a binary system containing 3 wt% of both SDBS and CTAB at different mixing ratios, corresponding to samples labeled A1–A11.

Table (5): Standard Gibbs free energy (ΔG°) values for 3 wt% SDBS:CTAB mixtures at different mixing ratios and temperatures.

Sample	CTAB 3%	SDBS 3%	ΔG° (kJ.mol^{-1})			
			283 K	293 K	303 K	313 K
A_1	10	0	4.291401	5.005461	5.855566	6.173528
A_2	9	1	3.257303	3.926521	4.506234	5.605884
A_3	8	2	0.211972	2.722852	3.934677	5.132611
A_4	7	3	2.25218 -	0.10835 -	3.017176	4.403206
A_5	6	4	1.22088 -	1.734726	3.701333	4.523724
A_6	5	5	0.11344 -	2.773832	4.015552	4.715154
A_7	4	6	1.350414	3.366461	4.373291	4.953533
A_8	3	7	2.335298	3.893379	4.860498	5.440295
A_9	2	8	3.453932	4.453941	5.541983	5.688702
A_{10}	1	9	4.303311	5.188344	5.838323	5.959869
A_{11}	0	10	4.733937	5.467475	6.18733	6.36647

From the analysis of the data presented in Table (5), it is observed that the standard Gibbs free energy (ΔG°) values increase (i.e., become less negative) with increasing temperature. This trend is accompanied by a noticeable decrease in viscosity values [35]. This behavior indicates a reduced tendency of the system to form wormlike micelles at higher temperatures, which can be attributed to the weakening of intermolecular attractive forces and reduced aggregation of surfactant molecules [36]. The

results further show that at 283 K and a mixing ratio of 7:3 (SDBS:CTAB), the standard Gibbs free energy value is −2.25218 kJ·mol^{-1}, indicating that micelle formation in this system is a spontaneous process. This indicates that, under these conditions, intermolecular interactions are sufficiently strong to favor self-assembly and reduce the free energy of the system.

Enthalpy (ΔH) of SDBS:CTAB Mixtures at Different Mixing Ratios

The enthalpy change (ΔH) associated with wormlike micelle formation was calculated using Equation (4), based on the Van't Hoff approach by plotting ln(η) versus the reciprocal of temperature (1/T in Kelvin) [37]. The slope of the linear relationship corresponds to (−ΔH/R), where R is the universal gas constant (8.314 J·mol^{-1}·K^{-1}). **Figs** (10-14), illustrate the determination of the slope for selected samples (A1, A2, A4, A5, and A11), respectively. The calculated values were subsequently summarized in Table (6).

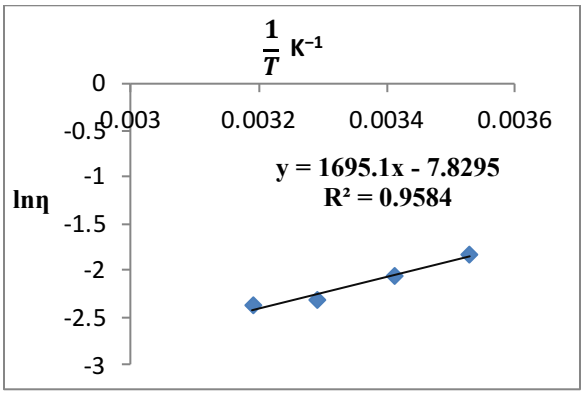

Fig (10): Relationship between ln(η) and (1/T) for the calculation of enthalpy of sample (A1).

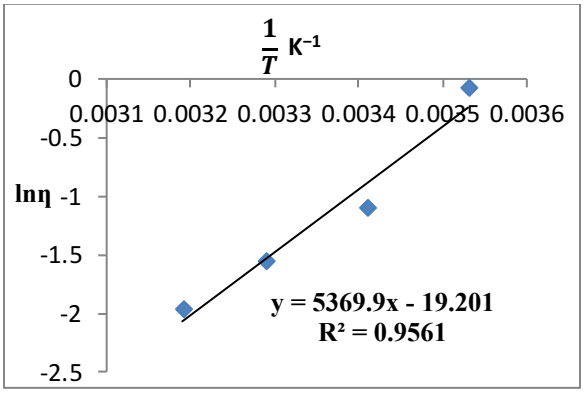

Fig (11): Relationship between ln(η) and (1/T) for the calculation of enthalpy of sample (A2).

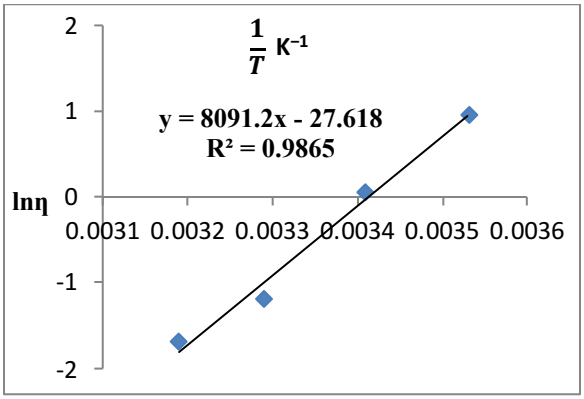

Fig (12): Relationship between ln(η) and (1/T) for the calculation of enthalpy of sample (A4).

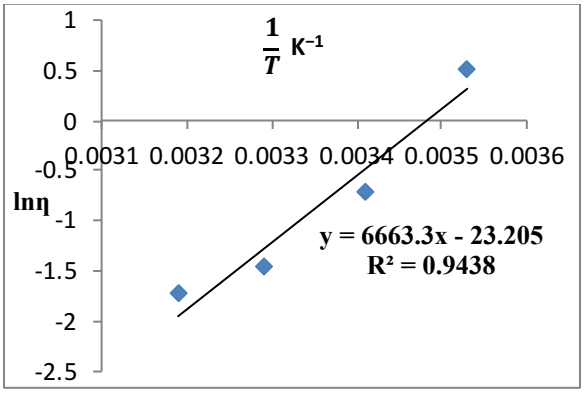

Fig (13): Relationship between ln(η) and (1/T) for the calculation of enthalpy of sample (A5).

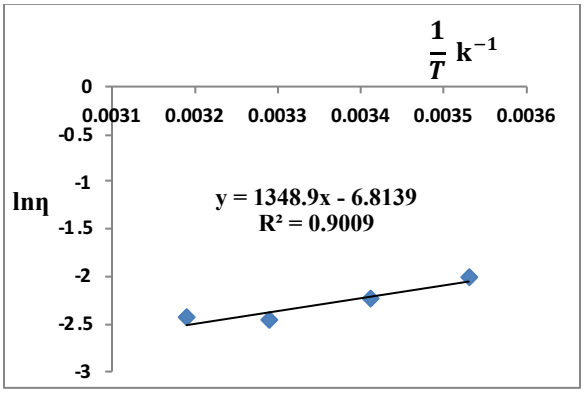

Fig (14): Relationship between ln(η) and (1/T) for the calculation of enthalpy of sample (A11).

Table (6): Enthalpy (ΔH) values for CTAB:SDBS mixtures at different mixing ratios and temperatures.

Sample	SDBS 3%	CTAB 3%	Slope	ΔH (kJ.mol^{-1})	R^2
A_1	0	10	1695.1	- 14.093	0.954
A_2	1	9	2162.6	- 17.979	0.961
A_3	2	8	5369.9	- 44.645	0.956
A_4	3	7	8091.2	- 67.270	0.986
A_5	4	6	6663.3	- 55.398	0.943
A_6	5	5	5349.5	- 44.475	0.901
A_7	6	4	3846.4	- 31.979	0.918
A_8	7	3	3206.0	- 26.654	0.947
A_9	8	2	2246.2	- 18.674	0.908
A_{10}	9	1	1403.3	- 11.667	0.849
A_{11}	10	0	1348.9	- 11.214	0.901

The standard enthalpy (ΔH) values, as presented in Table (6) for samples A1–A11 at different temperatures, were found to be negative, indicating that the mixing process of the surfactants CTAB and SDBS is an exothermic process [38]. This behavior reflects the presence of strong attractive interactions between the molecules, particularly electrostatic interactions between oppositely charged head groups, as well as hydrophobic interactions among hydrocarbon chains in the aqueous medium. These interactions promote molecular aggregation in order to reduce disruption of the water structure and decrease the overall Gibbs free energy of the system, thereby facilitating spontaneous self-assembly and micelle formation. Consequently, energy is released during the aggregation process.

Furthermore, the results revealed strong linear relationships in the thermodynamic analysis, with high correlation coefficients observed for several samples such as A1, A2, A4, A5, and A11, among others [39].

Entropy (ΔS°) of SDBS:CTAB Mixtures at Different Mixing Ratios and Temperatures

The standard entropy (ΔS°) values for the micellar system were calculated using Equation (5). Table (7) presents the ΔS° values for CTAB:SDBS surfactant mixtures at different mixing ratios, corresponding to samples A1–A11 and evaluated at various temperatures.

Table (7): Standard entropy (ΔS°) values for CTAB:SDBS surfactant mixtures at different mixing ratios and temperatures.

Sample Code	CTAB 3%	SDBS 3%	ΔS° (J.mol^{-1}.K^{-1}) 283 K	293 K	303 K	313 K
A_1	10	0	- 49.787	- 48.091	- 46.508	- 45.023
A_2	9	1	- 63.510	- 61.346	- 59.325	- 57.434
A_3	8	2	- 157.675	- 152.305	- 147.284	- 142.585
A_4	7	3	- 237.570	- 229.473	- 221.914	- 214.832
A_5	6	4	- 195.647	- 188.983	- 182.756	- 176.922
A_6	5	5	- 157.074	- 151.726	- 146.725	- 142.042
A_7	4	6	- 112.945	- 109.099	- 105.503	- 102.136
A_8	3	7	- 94.144	- 90.938	- 87.941	- 85.135
A_9	2	8	- 65.966	- 63.719	- 61.621	- 59.653
A_{10}	1	9	- 41.219	- 39.816	- 38.505	- 37.276
A_{11}	0	10	- 39.623	- 38.274	- 37.014	- 35.833

The results presented in Table (7) indicate that the standard entropy (ΔS°) values were negative at all studied temperatures. This behavior can be attributed to the structural nature of surfactant molecules, which consist of two main components: a hydrophobic hydrocarbon tail and a hydrophilic polar head group [40]. In aqueous media, the nonpolar hydrocarbon chains disrupt the ordered structure of surrounding water molecules, forcing water molecules to reorganize themselves in a more ordered arrangement around these hydrophobic segments to minimize the free energy of the system. This reorganization leads to a reduction in system randomness, and consequently a decrease in entropy [41]. During micelle formation, the hydrophobic tails

aggregate in the core of the micelle, away from water, while the polar head groups remain in contact with the aqueous environment. This structural arrangement reduces the degrees of freedom of molecules within the micellar assembly, leading to a decrease in the entropy of the system. However, this process is accompanied by the release of structured water molecules that were previously ordered around the hydrocarbon chains, which increases the randomness of these water molecules. Therefore, the overall entropy change represents a balance between two opposing effects: (i) a decrease in entropy due to the formation of ordered micellar structures, and (ii) an increase in entropy resulting from the release of water molecules and increased molecular freedom, in addition to the contribution of free ions present in the solution [29]. The results also show a slight increase in entropy with increasing temperature, which can be attributed to enhanced molecular motion and increased degrees of freedom at higher thermal energy levels [42].

Activation Energy (Ea) of CTAB:SDBS Mixtures at Different Mixing Ratios

The activation energy (Ea) for the formation of wormlike micelles in the binary surfactant system (CTAB:SDBS) at different mixing ratios was calculated using the Arrhenius equation [43]. This was achieved by plotting viscosity (η) against the reciprocal of absolute temperature (1/T), as described in Equation (6) The calculated values were summarized in Table (8)

Table (8): Activation energy (Ea) values for CTAB:SDBS surfactant mixtures at different mixing ratios.

Sample Code	SDBS 3%	CTAB 3%	Slope	Ea (kJ.mol^{-1})	R^2
A_1	0	10	2.0829	0.017	0.944
A_2	1	9	3.8129	0.031	0.987
A_3	2	8	21.707	0.180	0.821
A_4	3	7	71.121	0.591	0.885
A_5	4	6	42.542	0.353	0.792
A_6	5	5	24.744	0.205	0.769
A_7	6	4	11.729	0.097	0.822
A_8	7	3	7.0923	0.058	0.872

A_9	8	2	2.0829	0.017	0.944
A_{10}	9	1	3.8129	0.031	0.987
A_{11}	10	0	21.707	0.180	0.821

The results presented in Table (8) show well-defined linear relationships with high correlation coefficients, indicating the suitability of the applied model for describing the temperature dependence of viscosity in the studied system. The calculated activation energy (Ea) values for the CTAB:SDBS mixtures revealed that the highest value was obtained at a mixing ratio of 7:3, reaching 0.591 $kJ \cdot mol^{-1}$. This effect is attributed to formation of long and highly entangled wormlike micelles at this specific ratio, which increases internal flow resistance and therefore requires higher energy for molecular motion and flow [44]. From a physical standpoint, relatively high activation energy values indicate the presence of well-organized micellar structures, where viscosity increases due to micellar entanglement and the formation of a dynamic, polymer-like network. Several studies have reported that binary surfactant systems composed of oppositely charged species tend to form such structures at specific mixing ratios, resulting in a significant increase in both viscosity and activation energy [45]. Moreover, the application of the Arrhenius equation in viscosity analysis is widely recognized as an effective approach for characterizing micellar systems, as it provides a quantitative understanding of the effect of temperature on flow dynamics and micellar structural organization [46].

Viscosity Measurements and Thermodynamic Parameters of CTAB:SDBS Mixtures with Different Amoxicillin Concentrations

The effect of incorporating amoxicillin (AMO) at different concentrations (200, 100, 50, and 25 ppm) on the viscosity of the CTAB:SDBS (7:3) surfactant mixture was investigated at different temperatures (283, 293, 303, and 313 K). The obtained viscosity values for samples B1, B2, B3, and B4 were recorded and are presented in Table (9).

Table (9): Viscosity values of CTAB:SDBS (7:3) mixtures in the presence of different amoxicillin concentrations at various temperatures.

Sample	ctab	sdbs	Conc.	η(pa.s)× 10^2			
	3%	3%	AMO	283 K	293 K	303 K	313 K
B_1	7	3	25	0.02648	0.01075	0.00303	0.00142
B_2	7	3	50	0.02799	0.01089	0.00318	0.00159
B_3	7	3	100	0.02902	0.01140	0.00336	0.00178
B_4	7	3	200	0.03251	0.01167	0.00360	0.00212

The results presented in Table (9) indicate a clear increase in viscosity with increasing amoxicillin concentration in the CTAB:SDBS surfactant system. The data further show that viscosity decreases with increasing temperature [47]. while it increases with increasing solution concentration, which is a typical behavior observed in colloidal systems and surfactant-containing solutions. The highest viscosity value was recorded for sample (B4) at 283 K and a concentration of 200 ppm of amoxicillin, whereas the lowest viscosity value was observed for sample (B1) at 313 K and 25 ppm. The decrease in viscosity with increasing temperature is attributed to the increase in molecular kinetic energy, which weakens intermolecular attractive forces and reduces intermolecular cohesion. This enhances molecular mobility and decreases resistance to flow [48].On the other hand, the increase in viscosity with increasing concentration is attributed to the higher number of interacting molecules in the system, which enhances intermolecular interactions and promotes the formation of more complex structures within the solution. In this context, the observed increase in viscosity can be explained by the formation of hydrogen bonds between the hydroxyl groups of amoxicillin molecules and the polar sulfonate groups ($-OSO_3^-$) of sodium dodecylbenzene sulfonate (SDBS), thereby strengthening the interactions between system components.Moreover, these interactions may disrupt the electrostatic attraction between the oppositely charged head groups of SDBS and CTAB [49]. , contributing to the formation of more complex micellar structures such as wormlike micelles. These structures are known to significantly increase viscosity due to their entanglement and the formation of transient, polymer-like networks within the solution [50]. These findings are consistent with previous reports, which have reported that mixed ionic surfactant systems with oppositely charged species exhibit a significant increase in viscosity due to the formation of extended and highly entangled micellar structures, particularly in the

presence of drug molecules capable of forming hydrogen bonds or electrostatic interactions [51].

Standard Gibbs Free Energy (ΔG°) of CTAB:SDBS Mixtures at 7:3 Ratio in the Presence of Amoxicillin at Different Concentrations and Temperatures

The standard Gibbs free energy (ΔG°) of the surfactant mixture at a 7:3 (SDBS:CTAB) ratio was calculated in the presence of different concentrations of amoxicillin at various temperatures (283, 293, 303, and 313 K), using Equation (2). The calculated values are summarized in Table (10).

Table (10): Standard Gibbs free energy (ΔG°) values for CTAB:SDBS (7:3) mixtures in the presence of different amoxicillin concentrations at various temperatures.

Sample	ctab	sdbs	Conc.	ΔG° (kJ.mol^{-1})			
	3%	3%	AMO	283 K	293 K	303 K	313 K
B_1	7	3	25	- 2.292	- 0.177	3.083	5.072
B_2	7	3	50	- 2.423	- 0.208	3.034	4.979
B_3	7	3	100	- 2.508	- 0.319	2.904	4.163
B_4	7	3	200	- 2.775	- 0.376	2.384	3.835

From the data presented in Table (10), it is observed that an increase in amoxicillin concentration is accompanied by a decrease in the standard Gibbs free energy (ΔG°) at a constant temperature, which in turn indicates an enhancement in micelle formation. At 283 K and a concentration of 200 ppm of amoxicillin, the ΔG° value reached −2.775 kJ·mol⁻¹, suggesting a higher tendency for the system to form stable micellar structures. This behavior reflects the thermodynamic driving forces governing aggregation processes in pharmaceutical colloidal systems [52].

Enthalpy (ΔH) of CTAB:SDBS Mixtures (7:3) in the Presence of Amoxicillin at Different Concentrations and Temperatures

The enthalpy change (ΔH) for the surfactant system at a 7:3 (SDBS:CTAB) ratio in the presence of different concentrations of amoxicillin was determined at various temperatures (283, 293, 303, and 313 K). The calculations were performed using the Van't Hoff method (Equation 1.3), by

plotting ln(η) versus the reciprocal of absolute temperature (1/T in Kelvin) (37). The slope of the linear relationship corresponds to (−ΔH/R), where R is the universal gas constant (8.314 J·mol^{-1}·K^{-1}). **Figs** (15-18) illustrate the determination of the slope for samples B4, B3, B2, and B1, respectively. The calculated values were summarized in Table (11). The obtained enthalpy values indicate that micelle formation in the presence of different concentrations of amoxicillin is an exothermic process.

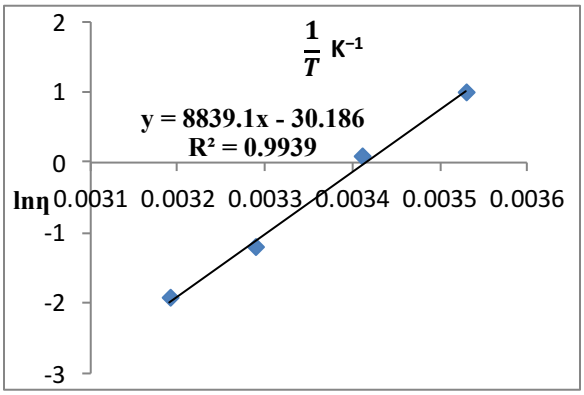

Fig (15): Relationship between ln(η) and (1/T) for the calculation of enthalpy of sample (B1).

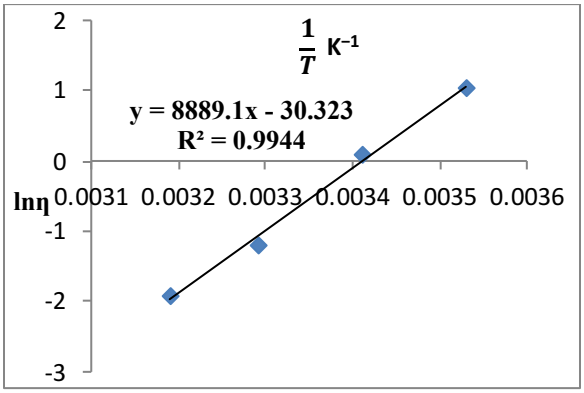

Fig (16): Relationship between ln(η) and (1/T) for the calculation of enthalpy of sample (B2).

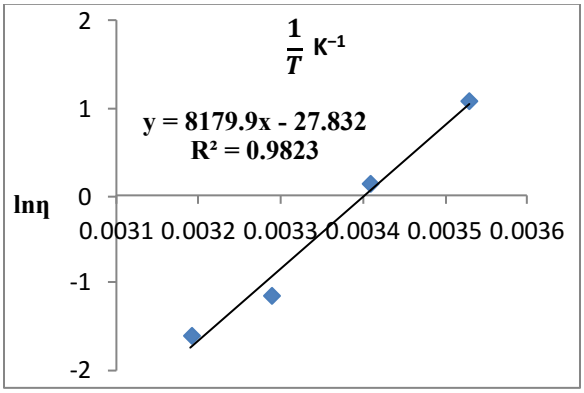

Fig (17): Relationship between ln(η) and (1/T) for the calculation of enthalpy of sample (B3).

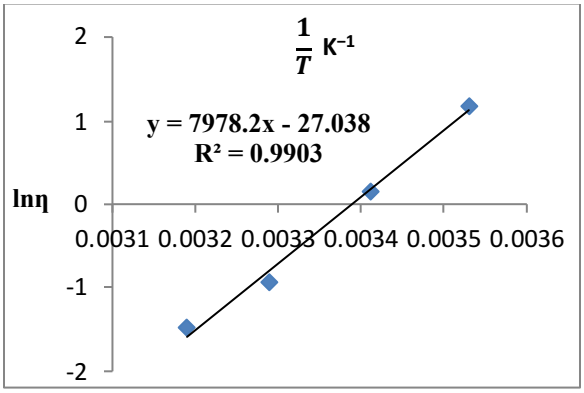

Fig (18): Relationship between ln(η) and (1/T) for the calculation of enthalpy of sample (B4).

Table (11): Enthalpy (ΔH) values for CTAB:SDBS (7:3) mixtures in the presence of different amoxicillin concentrations at various temperatures.

Sample Code	SDBS 3%	CTAB 3%	Conc. AMO (ppm)	Slope	ΔH (kJ.mol^{-1})	R^2
B_1	3	7	25	8808.4	73.233 -	0.995
B_2	3	7	50	8638.8	71.823 -	0.995
B_3	3	7	100	8425.4	70.048 -	0.993
B_4	3	7	200	8240.9	68.514 -	0.989

Entropy (ΔS°) Calculation for CTAB:SDBS (7:3) Mixture in the Presence of Amoxicillin at Different Concentrations and Temperatures

The standard entropy (ΔS°) values for the CTAB:SDBS (7:3) surfactant system in the presence of different concentrations of amoxicillin and at various temperatures were calculated using Equation (5). The obtained results were summarized and presented in Table (12).

Table (12): Standard entropy (ΔS°) values for CTAB:SDBS (7:3) mixtures in the presence of different amoxicillin concentrations at various temperatures.

Sample	CTAB 3%	SDBS 3%	Conc. AMO	ΔS° (J.mol^{-1}.K^{-1}) 283 K	293 K	303 K	313 K
B_1	7	3	25	- 251.44	- 250.07	- 252.58	- 250.87
B_2	7	3	50	- 252.44	- 251.39	- 253.79	- 251.90
B_3	7	3	100	- 231.32	- 230.89	- 233.91	- 230.46
B_4	7	3	200	- 223.49	- 224.05	- 225.77	- 223.19

From Table (12), it is observed that the entropy (ΔS°) values increase at constant temperatures. This behavior may be attributed to the spontaneous formation of wormlike micelles or to the formation of hydrogen bonds between amoxicillin molecules and the surfactant molecules (SDBS) [53]. In addition, increasing the drug concentration alters the ionic strength of the solution, which may reduce intermolecular interactions and enhance the mobility of ions, leading to an overall increase in system randomness.

Activation Energy (Ea) of CTAB:SDBS (7:3) Mixture in the Presence of Amoxicillin at Different Concentrations and Temperatures

The activation energy (Ea) for the CTAB and SDBS mixture at a 7:3 ratio in the presence of amoxicillin (AMO) at different concentrations and temperatures (283, 293, 303, and 313 K) was calculated based on the Arrhenius equation (Equation 6) [54]. This was achieved by plotting the relationship between viscosity (η) and the reciprocal of absolute temperature (1/T). The calculated values were summarized in Table (13).

Table (13): Activation energy (Ea) values for CTAB:SDBS (7:3) mixtures in the presence of different amoxicillin concentrations at various temperatures.

Sample	SDBS 3%	CTAB 3%	Conc. AMO	Slope	Ea (kJ.mol^{-1})	R^2

			(ppm)			
B_1	3	7	25	8839.1	0.612	0.993
B_2	3	7	50	8889.1	0.646	0.994
B_3	3	7	100	8179.9	0.660	0.982
B_4	3	7	200	7978.2	0.724	0.990

It is observed from Table (13) that the highest activation energy value corresponds to sample (B4), reaching 0.724 kJ·mol^{-1}, which contains the highest concentration of amoxicillin. This increase can be attributed to the rise in viscosity, which reduces molecular mobility. As a result, drug molecules require higher energy to overcome the increased hindrance to motion, leading to an increase in the activation energy [55].**Fig** (19) illustrates the method used to determine the slope of the linear relationship (Ea/R), which is employed to calculate the activation energy (Ea) for sample (B4). The obtained plot exhibited good linearity with a high correlation coefficient, as representative examples.

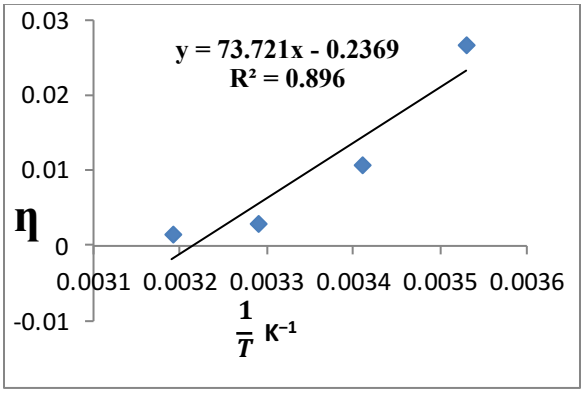

Fig (19): Relationship between η and (1/T) for the calculation of activation energy of sample (B4).

Viscosity Measurements and Thermodynamic Parameters of CTAB:SDBS (7:3) Mixture in the Presence of Amoxicillin, Thyme Extract, and Iron Oxide Nanoparticles

The ability of the binary surfactant system composed of CTAB and SDBS at a fixed ratio of 7:3 to form wormlike micelles was investigated in the presence of amoxicillin, thyme extract, and iron oxide nanoparticles (Fe_3O_4) at different concentrations (200, 100, 50, and 25 ppm) and temperatures

(283, 293, 303, and 313 K). The viscosity values obtained for the prepared samples (D1–D4) are presented in Table (14).

Table (14): Viscosity values of CTAB:SDBS (7:3) mixtures in the presence of different concentrations of amoxicillin, thyme extract, and iron oxide nanoparticles.

Sample	ctab 3%	sdbs 3%	Conc. AMO	Conc. Thyme	Conc. Fe_3O_4	η(pa.s)× 10^2 283 K	293 K	303 K	313 K
D_1	7	3	25	25	25	0.03328	0.01174	0.00414	0.00249
D_2	7	3	50	50	50	0.03469	0.01233	0.00450	0.00265
D_3	7	3	100	100	100	0.03559	0.01316	0.00485	0.00303
D_4	7	3	200	200	200	0.03721	0.01408	0.00538	0.00350

It is observed from Table (14) that the viscosity values increase with increasing concentration of iron oxide nanoparticles (Fe_3O_4) compared to the system before their addition. This increase can be attributed to the rise in the effective molecular weight of the mixture, which promotes the formation of larger molecular aggregates. In addition, the high specific surface area of the nanoparticles acts as a bridging network between micelles, facilitating their interconnection and continuity, which ultimately leads to an increase in viscosity [57،56]. **Fig (20)** illustrates the enhanced cross-linking of surfactant micelles in the presence of nanoparticles. It is also observed that temperature has a significant effect on the micellar structure of the surfactant mixture in the presence of nanoparticles, where an increase in temperature reduces micellar entanglement, leading to a decrease in viscosity [58].

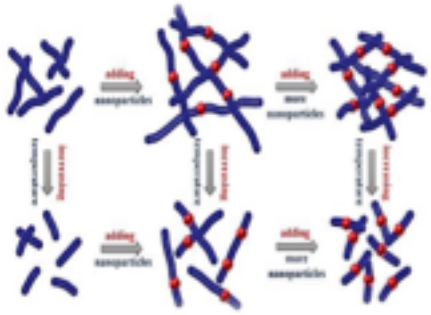

Fig (20): Increased micellar cross-linking of surfactant molecules.

Standard Gibbs Free Energy (ΔG°) Calculation for CTAB:SDBS (7:3) Mixture in the Presence of Thyme Extract, Amoxicillin, and Iron Oxide Nanoparticles

The standard Gibbs free energy (ΔG°) of the CTAB:SDBS surfactant system at a fixed ratio of 7:3 was calculated in the presence of different concentrations of amoxicillin, thyme extract, and iron oxide nanoparticles (Fe_3O_4) at concentrations of 200, 100, 50, and 25 ppm and at various temperatures (283, 293, 303, and 313 K). The calculations were performed using Equation (2), and the obtained results are presented in Table (15).

Table (15): Standard Gibbs free energy (ΔG°) values for CTAB:SDBS (7:3) mixtures in the presence of different concentrations of amoxicillin, thyme extract, and iron oxide nanoparticles.

Sample	CTAB 3%	SDBS 3%	Conc. AMO	Conc. Thyme	Conc Fe_3O_4	ΔG° (kJ.mol^{-1}) 283 K	293 K	303 K	313 K
D_1	7	3	25	25	25	2.830 -	0.392 -	2.222	3.611
D_2	7	3	50	50	50	2.928 -	0.511 -	2.012	3.449
D_3	7	3	100	100	100	2.988 -	0.670 -	1.821	3.104
D_4	7	3	200	200	200	3.093 -	0.834 -	1.560	2.731

From Table (15), it is observed that the standard Gibbs free energy (ΔG°) decreases with increasing concentration of iron oxide nanoparticles. The lowest value recorded was (−3.093 kJ·mol^{-1}) at 200 ppm of Fe_3O_4 in the presence of amoxicillin and thyme extract at 283 K. This behavior indicates an enhanced tendency of the system to form stable micellar structures, reflecting the thermodynamic driving forces governing aggregation in colloidal drug systems [52].

Enthalpy (ΔH) Calculation for CTAB:SDBS (7:3) Mixture in the Presence of Amoxicillin, Thyme Extract, and Iron Oxide Nanoparticles

The enthalpy change (ΔH) for the CTAB:SDBS surfactant system at a 7:3 ratio in the presence of different concentrations of amoxicillin, thyme extract, and iron oxide nanoparticles (200, 100, 50, and 25 ppm) was calculated using Equation (4) at temperatures of 283, 293, 303, and 313 K. This was done by determining the slope (−ΔH/R) from the linear plots obtained via the Van't Hoff relationship. **Figs** (21-24) illustrate the

procedure used to extract the slope of the linear relationship for the studied samples, and the obtained results were summarized in Table (16).

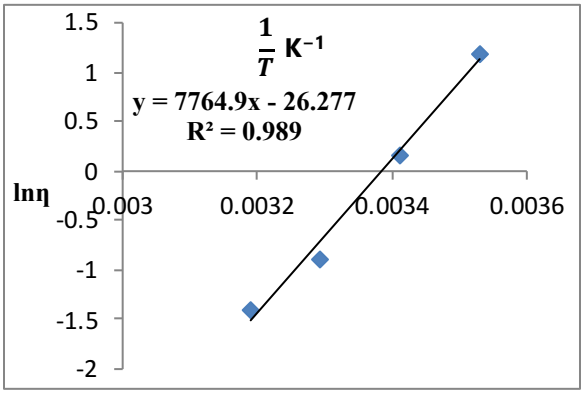

Fig (21): Relationship between ln(η) and (1/T) for the calculation of enthalpy of sample (D1).

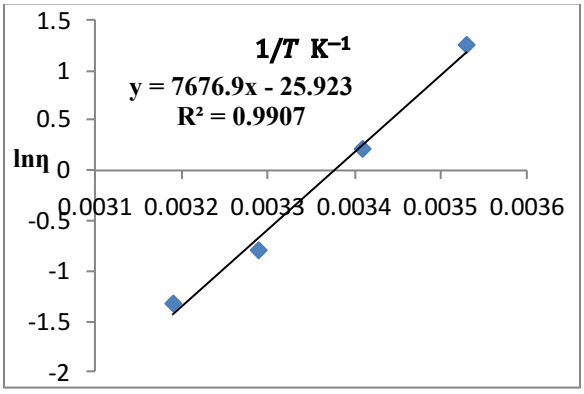

Fig (22): Relationship between ln(η) and (1/T) for the calculation of enthalpy of sample (D2).

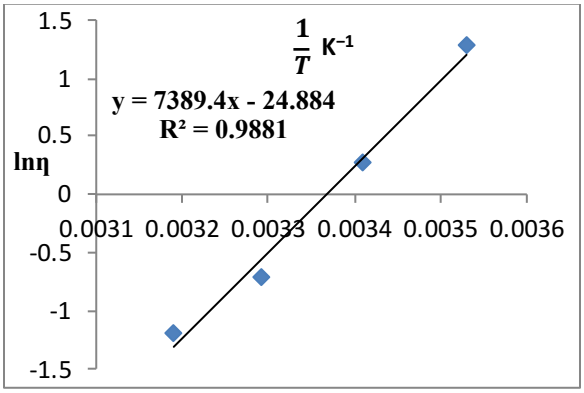

Fig (23): Relationship between ln(η) and (1/T) for the calculation of enthalpy of sample (D3).

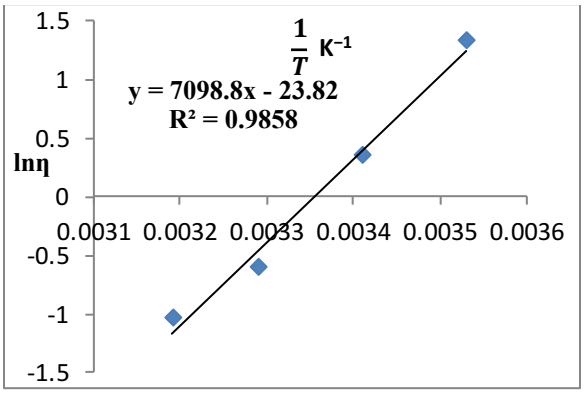

Fig (24): Relationship between ln(η) and (1/T) for the calculation of enthalpy of sample (D4).

Table (16): Enthalpy (ΔH) values for CTAB:SDBS (7:3) mixtures in the presence of different concentrations of amoxicillin, thyme extract, and iron oxide nanoparticles.

Sample	CTAB 3%	SDBS 3%	Conc. AMO	Conc. Thyme	Conc. Fe_3O_4	Slope	ΔH (kJ.mol^{-1})	R^2
D_1	7	3	25	25	25	7764.9	- 64.557	0.989
D_2	7	3	50	50	50	7676.9	- 63.825	0.990
D_3	7	3	100	100	100	7389.4	- 61.435	0.988
D_4	7	3	200	200	200	7098.8	- 59.019	0.985

Table (16) shows the enthalpy (ΔH) values for the CTAB:SDBS surfactant system in the presence of amoxicillin, thyme extract, and iron oxide nanoparticles. The results indicate that micelle formation is an exothermic process, as reflected by the negative enthalpy values (Exothermic). Moreover, the magnitude of ΔH increases with increasing concentration, with good correlation coefficients, indicating a consistent thermodynamic behavior across the studied systems [59].

Entropy (ΔS°) Calculation for CTAB:SDBS (7:3) Mixture in the Presence of Amoxicillin, Thyme Extract, and Iron Oxide Nanoparticles

The standard entropy change (ΔS°) associated with wormlike micelle formation for the CTAB:SDBS (7:3) system in the presence of different concentrations of amoxicillin, thyme extract, and iron oxide nanoparticles (200, 100, 50, and 25 ppm) was calculated using Equation (5). The

calculations were performed at the previously mentioned temperatures, and the obtained results are presented in Table (17).

Table (17): Standard entropy (ΔS°) values for CTAB:SDBS (7:3) mixtures in the presence of different concentrations of amoxicillin, thyme extract, and iron oxide nanoparticles.

Sample	CTAB 3%	SDBS 3%	Conc. AMO	Conc. Thyme	Conc. Fe_3O_4	ΔS° (kJ.mol^{-1}) 283 K	293 K	303 K	313 K
D_1	7	3	25	25	25	- 218.01	- 218.87	- 220.28	- 217.68
D_2	7	3	50	50	50	- 215.07	- 215.97	- 217.18	- 214.83
D_3	7	3	100	100	100	- 206.41	- 207.28	- 208.66	- 206.10
D_4	7	3	200	200	200	- 197.51	- 198.48	- 199.83	- 197.19

From Table (17), it is observed that the entropy (ΔS°) values are negative, and the increase in disorder is limited, which is mainly attributed to the spontaneous formation of micelles. In the ternary system consisting of ionic surfactants, the drug, plant extract, and iron oxide nanoparticles, micellization occurs in a highly ordered manner, leading to a reduction in system randomness [60]. Therefore, the overall entropy decreases as the structured micellar assemblies are formed.

Activation Energy (Ea) of CTAB:SDBS (7:3) Mixture in the Presence of Amoxicillin, Thyme Extract, and Iron Oxide Nanoparticles

The activation energy (Ea) for the CTAB and SDBS mixture at a 7:3 ratio was determined in the presence of different concentrations of amoxicillin, thyme extract, and iron oxide nanoparticles (200, 100, 50, and 25 ppm) at temperatures of 283, 293, 303, and 313 K. The calculations were based on the Arrhenius equation (Equation 1.5) (43), by plotting the relationship between viscosity (η) and the reciprocal of absolute temperature (1/T). The obtained results are presented in Table (18).

Table (18): Activation energy (Ea) values for CTAB:SDBS (7:3) mixtures in the presence of different concentrations of amoxicillin, thyme extract, and iron oxide nanoparticles.

Sample	SDBS 3%	CTAB 3%	Conc. AMO	Conc. Thyme	Conc. Fe_3O_4	Slope	Ea (kJ.mol^{-1})	R^2
D_1	3	7	25	25	25	88.929	0.7393	0.855
D_2	3	7	50	50	50	92.465	0.7687	0.857
D_3	3	7	100	100	100	94.275	0.7838	0.862

D_4	3	7	200	200	200	97.683	0.8121	0.864

From Table (18), it is observed that the activation energy (Ea) reaches its highest value compared to the previously obtained systems prior to the addition of iron oxide nanoparticles, particularly at the highest concentration (200 ppm). This behavior can be attributed to the increase in viscosity induced by the presence of the nanoparticles, which reduces molecular mobility. Consequently, drug molecules require higher energy to overcome the increased flow resistance, leading to an increase in activation energy [61]. **Fig (25)** illustrates the method used to determine the slope of the linear relationship (Ea/R) for calculating the activation energy of sample (D4). The obtained plot exhibited a clear linear relationship with a good correlation coefficient, confirming the applicability of the Arrhenius model in describing the temperature-dependent behavior of the system.

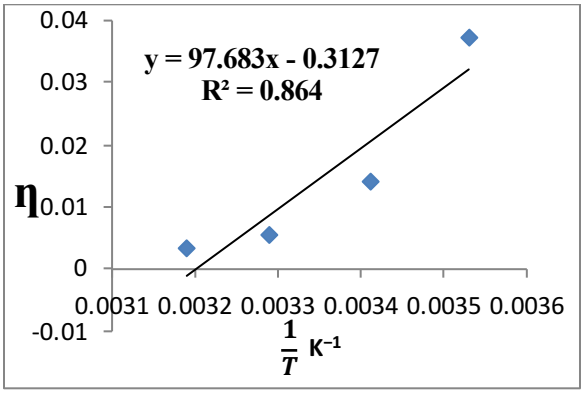

Fig (25): Relationship between η and (1/T) for the calculation of activation energy of sample (D4).

Zeta potential analysis

To further support micelle formation beyond viscosity measurements, zeta potential analysis was considered. As shown in Fig. 26, the zeta potential values decreased progressively with increasing surfactant concentration and exhibited a sharp transition near the critical micelle concentration (CMC). This behavior indicates the formation of mixed micellar aggregates and confirms the electrostatic interactions between the cationic CTAB and anionic SDBS surfactants. Moreover, the transition from positive to highly negative zeta potential values after the CMC suggests

charge reversal and the formation of stable colloidal micellar structures. The high absolute zeta potential values (approximately −40 to −55 mV) indicate good colloidal stability due to strong electrostatic repulsion between micelles.

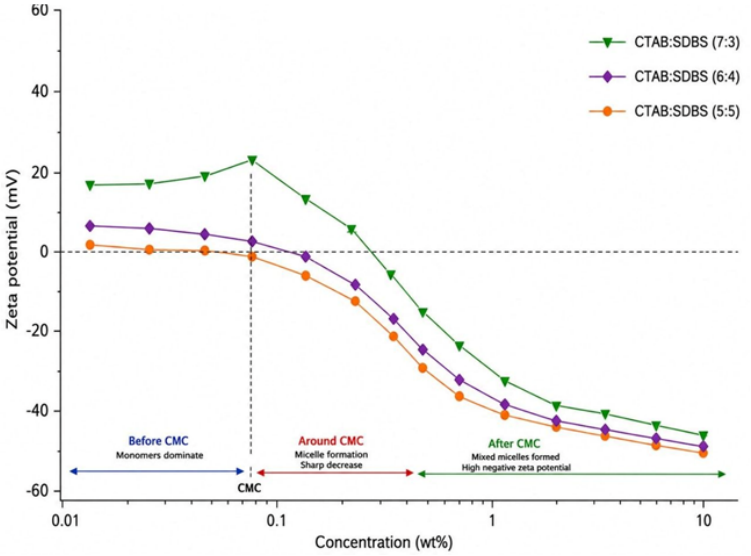

Fig (26). Illustrate Zeta potential vs concentration for CTAB:SDBS in Surfactant System

Conclusions

Based on the obtained results and discussion, the following conclusions can be drawn:

1. The highest viscosity of the CTAB:SDBS surfactant mixture was observed at the mixing ratio of 7:3.
2. Increasing temperature leads to a decrease in the viscosity of all studied systems, including:
    - CTAB:SDBS
    - CTAB:SDBS in the presence of amoxicillin
    - CTAB:SDBS in the presence of amoxicillin, thyme extract, and iron oxide nanoparticles
3. The viscosity of the studied systems increases with increasing concentrations of amoxicillin, thyme extract, and iron oxide

nanoparticles. This is attributed to strong hydrogen bonding interactions, in addition to the role of nanoparticles acting as a bridging network between micelles, enhancing their entanglement and interconnection.

4. The viscosity of the CTAB:SDBS system in the presence of amoxicillin, thyme extract, and iron oxide nanoparticles is higher than that of the CTAB:SDBS system containing only amoxicillin.
5. Most micelle formation processes are spontaneous ($\Delta G° < 0$), exothermic ($\Delta H < 0$), and associated with a decrease in entropy ($\Delta S° < 0$), indicating the formation of more ordered and thermodynamically stable micellar structures.

References

[1] M. G. W. Gangurde and B. A. Shingade, *Advances in Nanoscience and Nanotechnology*. Addition Publishing House, 2025.

[2] S. Pedalino, B. E. Ramírez-Galindo, R. Ferstl, K. Hornberger, M. Arndt, and S. Gerlich, "Probing quantum mechanics with nanoparticle matter-wave interferometry," *Nature*, vol. 649, no. 8098, pp. 866–870, 2026.

[3] K. Zheng *et al.*, "Ultra Strong and Tough Bio-Based Polyurethane Elastomers with Rigid-Flexible Hybrid Soft Segment Supramolecular Cross-linked Networks," *Adv. Funct. Mater.*, vol. 36, no. 4, p. e09794, 2026.

[4] A. Yadav and S. Dutta, "Single-metal-atom-incorporated quantum dots and covalent organic frameworks: a comparison of quantum effects and electronics," *J. Mater. Chem. A*, vol. 13, no. 16, pp. 11159–11184, 2025.

[5] E. Aleebrahim-Dehkordi, A. Sheibaninia, and A. Ghasemi Pirbalouti, "Functional and Organic Foods in Enhancing the Oral and Dental Health and Hygiene—A Comprehensive Review," *Food Sci. Nutr.*, vol. 14, no. 2, p. e71433, 2026.

[6] A. Ngabirano, V. A. Yiga, and M. Lubwama, "Synthesis and characterization of mesoporous bio-silica nanoparticles developed from rice husks for oil spillage remediation," *Results Eng.*, p. 109369, 2026.

[7] P. D. V Surya, S. Sirohi, P. Vashist, and A. K. Nelapati, "Challenges and Future Direction of Nanotechnology in Biomedical Applications," in *Advanced Nanohybrids for Biomedical Applications*, CRC Press, 2026, pp. 177–194.

[8] A. Kumar, G. Patel, and K. P. Narayan, "Biodegradable Lipids and Surfactants: Next-Generation Drug Delivery for Cancer Therapeutics," in *Applications of Nanomaterials for Oncology*, IGI Global Scientific Publishing, 2026, pp. 1–34.

[9] H. Wennerström and D. F. Evans, *The colloidal domain: where physics, chemistry, biology, and technology meet*. John Wiley & Sons, 2026.

[10] E. Abdolrasheid, A. E. El-Tabey, A. M. El-Naggar, A. I. Hashem, N. M. Nasser, and A. M. Al-Sabagh, "Synthesis of new family of anionic/nonionic surfactant moieties based on mono maleate

derivatives and investigate their physical properties," *J. Dispers. Sci. Technol.*, vol. 47, no. 3, pp. 397–415, 2026.

[11] Q. Dinora, "ENHANCING THE BIOAVAILABILITY OF SOLID DOSAGE FORMS USING NANOTECHNOLOGY," *Mod. Educ. Dev.*, vol. 41, no. 2, pp. 191–196, 2026.

[12] Y. Zhu *et al.*, "Multifunctional nanocarrier drug delivery systems: from diverse design to precise biomedical applications," *Adv. Healthc. Mater.*, vol. 15, no. 2, p. e02178, 2026.

[13] Y. Meng, Y. Feng, X. Bai, Q. Yu, J. Zhou, and J. Wang, "Application of nanotechnology in agricultural sustainability: Absorption, translocation, and challenges of nanoparticles," *Curr. Plant Biol.*, vol. 42, p. 100492, 2025.

[14] T. Ma *et al.*, "Regulation mechanism of surfactant-SiO_2 nanoparticle compound on the mechanical property and microstructure of coal: Effect of the type of surfactant," *Powder Technol.*, p. 121459, 2025.

[15] A. R. Abubakar and M. Haque, "Preparation of medicinal plants: Basic extraction and fractionation procedures for experimental purposes," *J. Pharm. Bioallied Sci.*, vol. 12, no. 1, pp. 1–10, 2020.

[16] H. Y. El-Kassas, M. A. Aly-Eldeen, and S. M. Gharib, "Green synthesis of iron oxide (Fe3O4) nanoparticles using two selected brown seaweeds: characterization and application for lead bioremediation," *Acta Oceanol. Sin.*, vol. 35, no. 8, pp. 89–98, 2016.

[17] J. Choi, J. M. Kim, and K. S. Cho, "A Solid-Based Approach for Modeling Simple Yield-Stress Fluids: Rheological Transitions, Overshoot and Relaxation," *arXiv Prepr. arXiv2604.03467*, 2026.

[18] D. Kitto *et al.*, "Specific ion effects on ion transport in charged polymer membranes," *Sci. Adv.*, vol. 12, no. 11, p. eadx1214, 2026.

[19] K. Jin, P. Rychahou, D. W. Binzel, B. M. Evers, and P. Guo, "RNA-Micelles as Self-Assembling Structures for Efficient Co-Delivery of Synergistic siRNA and Nucleoside Analogues to Treat CRC Lung Metastasis," *Adv. Funct. Mater.*, p. e21863, 2026.

[20] O. Watts Moore *et al.*, "Optical Coherence Tomography Velocimetry for In-Line Processing: The Spherical-to-Wormlike Micelle Transition," *ACS Eng. Au*, vol. 5, no. 6, pp. 639–647, 2025.

[21] K. Ako, S. Elmarhoum, and C. D. Munialo, "The determination of the lower critical concentration temperature and intrinsic viscosity: The syneresis reaction of polymeric gels," *Food Hydrocoll.*, vol. 124, p.

107346, 2022.

[22] Z. Zhou *et al.*, "Innovative high-entropy strategy extending traditional metal substitution for optimizing prussian blue analogues in rechargeable batteries," *SusMat*, vol. 5, no. 2, p. e265, 2025.

[23] T. Purcell, G. Delaplace, A. Riaublanc, M. Demême, A. Derensy, and G. Della Valle, "A general viscosity model for high moisture extrudates of pea protein isolates/gluten blend," *Phys. Fluids*, vol. 37, no. 3, 2025.

[24] J. Gómez-Márquez, "The Origin of Life and Cellular Systems: A Continuum from Prebiotic Chemistry to Biodiversity," *Life*, vol. 15, no. 11, p. 1745, 2025.

[25] S. Anand, "Transport, Energetics, and Self-Organization in Non-Equilibrium Systems," 2026, *New York University*.

[26] X.-G. Wang, D.-H. Liu, H.-B. Cheng, Q. Luo, K. Tang, and D.-Y. Zhu, "Thickening characteristics and conformance control mechanism of CO2-responsive fluid during CO2 flooding," *Pet. Sci.*, 2026.

[27] A. Banerjee, B. Debnath, D. Ray, and B. Das, "Single Molecular, Self-Assembly and Adsorption Properties of N-Tetradecyl-N-Methylmorpholinium Bromide in Aqueous Solutions," *J. Surfactants Deterg.*, vol. 28, no. 5, pp. 1149–1163, 2025.

[28] V. L. Dharmaraj, Y. Fang, and M. V Tirrell, "Effect of Polymer Structure on the Thermodynamics of Polyelectrolyte Complex Micelle Formation," *Macromolecules*, 2026.

[29] A. Chen, T. Zhang, W. Liu, J. Xie, and Q. Zhang, "Impact of temperature on interfacial behavior and rheology of oleate-mediated apatite/dolomite pulp: Linking molecular interactions to macroscopic viscosity," *Colloids Surfaces A Physicochem. Eng. Asp.*, p. 138053, 2025.

[30] M. K. Hasan, T. Khandaker, M. S. Hossain, A. B. M. Ibrahim, and S. Kawaguchi, "Determination of Critical Micelle Concentration of Amphiphilic Surfactants: A Comprehensive Review," *Anal. Chem.*, 2026.

[31] F. Ahmed and L. P. Chamorro, "On Bio-Inspired Strategies for Flow Control, Fluid–Structure Interaction, and Thermal Transport," *Biomimetics*, vol. 11, no. 2, p. 143, 2026.

[32] M. Basu, S. D. Choudhury, S. Kumar, B. Dutta, and S. B. Shelar, "Exploring thermodynamic stability and microenvironment of dilute

bile salt based ‘catanionic’assemblies of relevance to drug delivery,” *Colloid Polym. Sci.*, pp. 1–18, 2026.

[33] P. Vainikka and K. J. Edler, “Surfactant self-assembly and micelle elongation in reline: structural basis and driving forces,” *Philos. Trans. R. Soc. A Math. Phys. Eng. Sci.*, vol. 384, no. 2316, 2026.

[34] C. Panda, S. Kumar, S. Gupta, and L. M. Pandey, “Shear-Induced Structural Changes Drive Amorphous Aggregate Formation of Human Insulin,” *Proteins Struct. Funct. Bioinforma.*, vol. 93, no. 12, pp. 2074–2090, 2025.

[35] B.-W. Li *et al.*, “Optimization of glycyrrhizic acid-assisted green extraction of curcumin from Curcuma longa: water solubility, bioactivity, and stability,” *J. Mol. Liq.*, p. 128652, 2025.

[36] D. Mohanraj, A. Jamdagneya, A. Varadharajan, and W. E. Acree, “Common errors made in the mathematical representation of experimental data using the van’t Hoff and modified Apelblat equations and their effect on calculated thermodynamic quantities,” *Phys. Chem. Liq.*, vol. 64, no. 1, pp. 171–185, 2026.

[37] G. C. TOFAN, B. Pricop, C. A. ŢUGUI, and A. A. Minea, “Experimental study on SDBS surfactant effect on titanium oxide water nanofluid properties,” *Alexandria Eng. J.*, vol. 141, pp. 132–137, 2026.

[38] G. Yue, L. Zhang, M. Li, W. Tan, and J. Zhang, “Experimental study on thermodynamic and rheological properties of fly ash cenospheres concrete during high temperature processes,” *Constr. Build. Mater.*, vol. 458, p. 139558, 2025.

[39] A. A. Bautista-Solano, G. Dávila-Ortiz, M. de J. Perea-Flores, and A. L. Martínez-Ayala, “A comprehensive review of niosomes: composition, structure, formation, characterization, and applications in bioactive molecule delivery systems,” *Molecules*, vol. 30, no. 17, p. 3467, 2025.

[40] L. Pašalić *et al.*, “Peptide interaction with mixed lipid bilayers alters packing and hydrocarbon chain conformations,” *J. Liposome Res.*, vol. 35, no. 4, pp. 548–565, 2025.

[41] G. Zhang, Y. Zheng, W. Kang, H. Yang, and B. Sarsenbekuly, “Micelle Thermodynamic Properties and Interaction Behavior of the Prepared Extended Amphoteric Surfactant with Gemini Cationic Surfactants,” *Langmuir*, vol. 42, no. 8, pp. 6048–6059, 2026.

[42] Y. Chung and W. H. Green, "New modified Arrhenius equation to describe the temperature dependence of liquid phase reaction rates," *Chem. Eng. J.*, vol. 516, p. 163300, 2025.

[43] T. Rees-Crockford, E. Scullion, E. Khomenko, and Á. de Vicente, "The observational and numerical analysis of the Rayleigh–Taylor instability beneath a hedgerow prominence," *Astrophys. J.*, vol. 974, no. 1, p. 64, 2024.

[44] R. Suarez Lopez, "Simplifying Complexity: Harnessing Coarse-Grained Models to Study Intricate Systems," 2023.

[45] S. Li, M. Luo, A. B. Boldianu, and D. J. McClements, "Food-Grade Emulsion Gels as Nutrient Delivery Systems—Standardized Workflow for Fabrication, Characterization, and Application," *Gels*, vol. 12, no. 4, p. 298, 2026.

[46] R. Kashyap, K. Saha, and K. A. Subramanian, "Molecular dynamics simulation of the transport and structural properties for methanol-octane blends at engine-relevant conditions," *Int. J. Green Energy*, pp. 1–25, 2025.

[47] S. Jin, C. Xiao, H. Lu, and X. Deng, "Effects of extrusion temperature on structure and physicochemical properties of proso millet starch," *Int. J. Biol. Macromol.*, vol. 299, p. 140011, 2025.

[48] F. Hassan *et al.*, "Pharmaceutical and pharmacological evaluation of amoxicillin after solubility enhancement using the spray drying technique," *ACS omega*, vol. 7, no. 51, pp. 48506–48519, 2022.

[49] K. B. Shishkhanova, V. S. Molchanov, and O. E. Philippova, "Tuning of the Viscosity Maximum and the Temperature Effect on Wormlike Micelle Solutions Using Hydrotropic and Inorganic Salts," *Liquids*, vol. 5, no. 4, p. 28, 2025.

[50] L. Zakharova *et al.*, "Biomimetic supramolecular systems: noncovalent strategy in self-assembly, functional activity and drug delivery," *Biophys. Rev.*, pp. 1–18, 2025.

[51] R. Davis Jr, I. Duggal, N. A. Peppas, and A. K. Gaharwar, "Designing the next generation of biomaterials through nanoengineering," *Adv. Mater.*, vol. 37, no. 39, p. 2501761, 2025.

[52] R. Singh, J. Gurung, A. J. Gogoi, and A. K. Pulikkal, "Molecular interactions of cationic/anionic surfactants in presence of anionic antibiotic drug cloxacillin sodium at different temperatures: Micellization and thermodynamic studies," *J. Mol. Liq.*, vol. 395, p.

123807, 2024.

[53] M. H. Warsi, G. Varshney, R. Malviya, S. Kumar, S. B. Sridhar, and A. Zafar, "Characterization of Tragacanth Gum as Biomedical and Food Adjuvant: Determination of Temperature-Dependent Coefficients of Viscosity and Surface Tension," *Curr. Anal. Chem.*, 2025.

[54] H. Zhang, Y. Ruan, C. Rong, W. Xing, and X. Duan, "Molecular dynamics simulations of structure and dynamics of ionic solutions under Couette shear flow," *J. Chem. Phys.*, vol. 164, no. 10, 2026.

[55] T. Khandaker *et al.*, "Recent progress in gel catalysts: boosting efficiency for sustainable energy applications," *Catal. Sci. Technol.*, vol. 15, no. 5, pp. 1357–1389, 2025.

[56] S. Khan *et al.*, "Designing MOF-based green nanomaterials for enhanced pathogen resistance and pesticide degradation in tomato plants," *Environ. Sci. Nano*, vol. 12, no. 2, pp. 1186–1201, 2025.

[57] E. Warmbier-Wytykowska *et al.*, "How do the valency and radii of cations affect the rheological properties of aqueous solutions of zwitterionic and anionic surfactant mixtures?," *Langmuir*, vol. 41, no. 5, pp. 3561–3571, 2025.

[58] F. Z. Sache, F. Z. Batanaa, and B. Saidat, "Analytical study of codeine adsorption using a molecularly imprinted polymer prepared by Fenton-initiated polymerization," *Anal. Methods Environ. Chem. J.*, vol. 9, no. 1, pp. 32–49, 2026.

[59] F. A. S. Islam and M. A. N. Islam, "AI-driven integration of nanotechnology and green nanotechnology for sustainable energy and environmental remediation," *J. Eng. Res. Reports*, vol. 27, no. 7, pp. 260–311, 2025.

[60] J. Zhang *et al.*, "Electrolyte coordination environments in wide-temperature aqueous metal batteries: mechanisms and design strategies," *Chem. Sci.*, vol. 17, no. 3, pp. 1569–1582, 2026.